PAPER Special Section on Leading-Edge Technologies of Superconducting Measurement Systems

Low Leakage Current Nb-Based Tunnel Junctions with an Extra Top Al Layer

Mizuki IKEYA[†a)], **Takashi NOGUCHI**[††], **Takafumi KOJIMA**[††], *Members*, *and* **Takeshi SAKAI**[†], *Nonmember*

SUMMARY In this paper, we describe the fabrication of low leakage Superconductor/Insulator/Superconductor (SIS) junctions with a Nb/Al/AlO$_x$/Al/Nb structure. In other words, an extra Al layer was added onto the top of the insulator in a conventional Nb/Al/AlO$_x$/Nb junction. We measured the current and voltage (*IV*) characteristics of both the Nb/Al/AlO$_x$/Al/Nb and Nb/Al/AlO$_x$/Nb junctions at the temperature of liquid helium, and found that the sub-gap leakage current in the Nb/Al/AlO$_x$/Al/Nb junctions was much lower than that of the Nb/Al/AlO$_x$/Nb junctions. Our analysis of the *IV* characteristics indicates that the quality of the AlOx insulator used in the Nb/Al/AlOx/Al/Nb junction was close to ideal, while the insulator used in the Nb/Al/AlOx/Nb junction had possible defects. According to the scanning transmission electron microscope (STEM) images and energy-dispersive X-ray spectroscopy (EDX) analyses, it was evident that the Nb atoms diffused into the bottom electrode of the Nb/Al/AlO$_x$/Nb junction, while a smaller number diffused into the bottom electrode of the Nb/Al/AlO$_x$/Al/Nb junction. Therefore, we conclude that the extra Al layer effectively acted as a buffer layer that prevented the Nb atoms from diffusing into the insulator and bottom electrode. The presence of the top Al layer is expected to favorably improve the quality of junctions with a very high current density, and support the extension of the RF and IF bandwidths of SIS mixers.

key words: *SIS, junction, IV characteristic, sub-gap current, STEM, EDX*

1. Introduction

Superconductor/Insulator/Superconductor (SIS) mixers are commonly used in highly-sensitive receivers for radio telescopes at millimeter and submillimeter wavelengths, such as the Atacama Large Millimeter/submillimeter Array (ALMA) (e.g. [1]), which is a large radio interferometric telescope that consists of 66 antennas. The receiver installed on each antenna covers a radio frequency (RF) range of 35–950 GHz, which is divided into ten frequency bands. The ALMA has already provided us with very useful scientific results because of its superior performance.

In recent years, researchers have begun to study the development of receivers for future radio astronomy applications. One of the key issues being explored is the need for SIS mixers that have an extremely wide RF bandwidth, because this can be used to upgrade the current receivers as well as provide a foundation for the next generation of radio receivers. Mixers with a wide RF bandwidth enable us to achieve flatter performance independent of the RF frequency. Moreover, if two adjacent RF bands (e.g. ALMA bands 7 + 8) can be covered by a single receiver, then the number of receiver ports needed at the 4-K stage is reduced.

In order to extend the RF bandwidth of an SIS mixer, SIS junctions that are high quality and have a high critical current density (J_c) are necessary. The SIS junction can be approximately described by an equivalent circuit consisting of an R_n and C_j in parallel, where R_n and C_j are the normal state resistance and capacitance of the junction, respectively. Since the fractional bandwidth $\Delta f / f_c$ of the mixer is determined by the time constant $R_n C_j$ of the junction, and J_c is proportional to $1/(R_n C_j)$, SIS junctions with a higher J_c are essential for the development of receivers with very wide RF bandwidths.

In a high J_c SIS junction, the insulator layer is very thin. In the case of Nb/Al/AlO$_x$/Nb junctions, which are widely used in low-noise millimeter- and submillimeter-wave receivers in radio astronomy applications, the sub-gap leakage current has been observed to significantly increase in junctions where $J_c > 10$ kA/cm^2 [2]. This level of leakage current may be due to the presence of metallic channels or defects in the aluminum oxide layer because its thickness is too thin to uniformly cover the bottom Nb surface in high-current density junctions. In addition, lower valence niobium oxide may be produced during the deposition of the top Nb electrode, which may cause defects in the insulator and broaden the divergence of the density of the quasiparticle state at the gap energy, as shown in Fig. 1, particularly in junctions with a higher J_c.

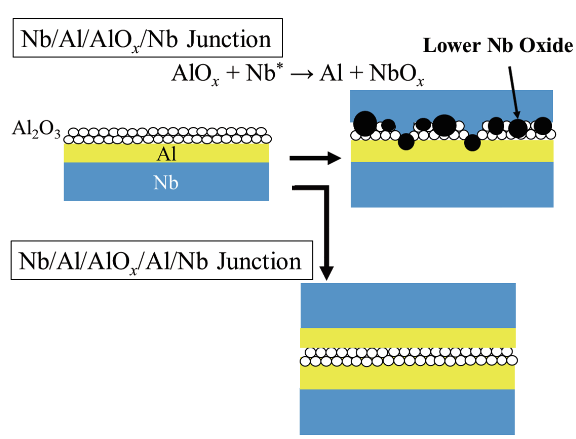

Fig. 1 Schematics of the junctions fabricated in this study showing the degradation of the AlO$_x$ barrier layer, and the method of reducing this degradation proposed in this paper.

Manuscript received July 10, 2016.
Manuscript revised December 10, 2016.
†The authors are with The University of Electro-Communications, Chofu-shi, 182–8585 Japan.
††The authors are with National Astronomical Observatory of Japan, Mitaka-shi, 181–8588 Japan.
a) E-mail: mizuki.ikeya@mail.uec.jp
DOI: 10.1587/transele.E100.C.291

Copyright © 2017 The Institute of Electronics, Information and Communication Engineers

On the other hand, Nb/Al/AlO$_x$/Al/Nb junctions, as shown in Fig. 1, are used in X-ray or terahertz detectors because of their low leakage features [3]. The top Al layer is expected to suppress not only the creation of metallic channels in the AlO$_x$ insulator, but also to suppress the growth of lower valence niobium oxides on the AlO$_x$ because of the chemical reaction between the Nb and AlO$_x$ during the deposition of the top Nb electrode. To understand the differences between these cases, we studied the electrical and structural properties of these two types of junctions in more detail.

2. Fabrication

Since the addition of a thick top Al layer (~20 nm) significantly reduces the gap voltage [4]–[6], the top Al layer should be thinner than ~20 nm. On the other hand, an Al layer that is too thin will not completely cover the surface of the AlO$_x$ insulator. For these reasons, we used a thickness of 10 nm for both the bottom and top Al layers of the Nb/Al/AlO$_x$/Al/Nb junction. The junction had a circular shape with a diameter of 3 μm.

The Nb/Al/AlO$_x$/Al/Nb multilayer was fabricated in a CS-200 ET (ULVAC) sputtering system without breaking a vacuum. The Nb layers were deposited with an Ar gas pressure of 1.0 Pa and a cathode DC current of 4.0 A. The Al layers were deposited with an Ar gas pressure of 1.0 Pa and a cathode DC current of 0.2 A. The oxidation of the surface of the bottom Al layer in order to form AlO$_x$ was performed by exposing the bottom Al film to an O_2 atmosphere with a pressure of 0.03 Pa for 30 min in a load-locked chamber. For comparison purposes, an Nb/Al/AlO$_x$/Nb junction with an Al layer thickness of 10 nm was also fabricated. To fabricate this junction, we adopted the same fabrication parameters, except that the oxidation pressure in this case was 0.15 Pa in order to achieve a current density that was as high as that of the Nb/Al/AlO$_x$/Al/Nb junction.

Figure 2 shows the transmission electron microscope (TEM) images of the cross sections of the two types of junctions. The thickness of both the bottom and top Al layers in the two types of junctions shown in Fig. 2 are approximately 10 nm.

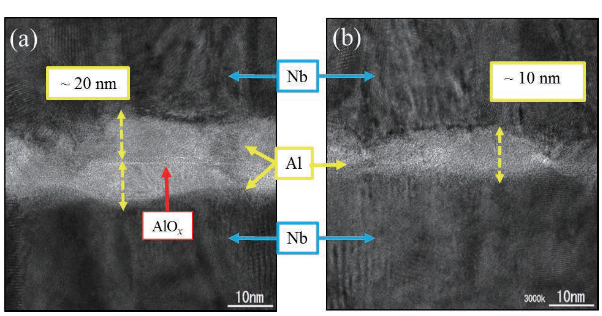

Fig. 2 Transmission Electron Microscope (TEM) images of the (a) Nb/Al/AlO$_x$/Al/Nb and (b) Nb/Al/AlO$_x$/Nb junctions.

3. *IV* Characteristics

We measured the *IV* curve of each junction at the temperature of liquid helium. A magnetic field was applied in order to suppress the DC Josephson current. Figure 3 shows the measured *IV* curves of the two types of junctions. Based on the junction size and the normal resistance, J_c was estimated to be ~8 kA/cm^2 in both of the junctions.

In Fig. 3, it can be seen that the sub-gap leakage current in the Nb/Al/AlO$_x$/Al/Nb junction was lower than that of the Nb/Al/AlO$_x$/Nb junction, although their gap voltages were similar. This strongly indicates that the top Al layer in the Nb/Al/AlO$_x$/Al/Nb junction played a significant role in suppressing the sub-gap leakage current. In the next section, we investigate the characteristics of the Nb/Al/AlO$_x$/Al/Nb junction in more detail.

4. Analysis of the *IV* Characteristics

In this section, we follow the method to fit the DC *IV* curves that was reported by Noguchi *et al.* [7]. The quasiparticle tunnel current at the SIS junction can be expressed as [8]:

$$I_T(V) = A \int N_u(E - eV) N_l(E) \{f_u(E - eV) - f_l(E)\} dE, \quad (1)$$

where A is a constant, E is the energy, V is the voltage, $N_u(E)$ and $N_l(E)$ are the density of states for the upper and lower electrodes, respectively, and $f_u(E)$ and $f_l(E)$ are the fermi function of the upper and lower electrodes, respectively. The values for the terms $N_{u,l}(E)$ and $f_{u,l}(E)$ can be expressed as:

$$N_{u,l}(E) = \mathrm{Re}\left[\frac{|E|}{\sqrt{E^2 - \Delta_{u,l}{}^2}}\right], \quad (2)$$

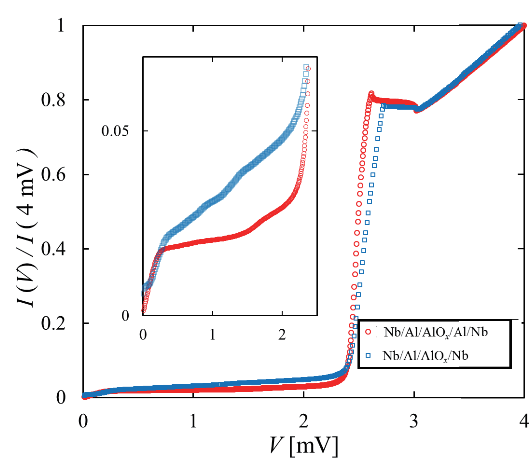

Fig. 3 Comparison between the measured *IV* characteristics of the Nb/Al/AlO$_x$/Nb junction (blue squares) and that of the Nb/Al/AlO$_x$/Al/Nb junction (red circles). The DC Josephson current was suppressed by applying a magnetic field.

and

$$f_{u,l}(E) = \frac{1}{\exp\left(\frac{E}{k_B T}\right)} + 1, \tag{3}$$

respectively, where Δ_u and Δ_l are the gap energy of the upper and lower electrodes, respectively, k_B is the Boltzmann constant, and T is the temperature. In order to realistically simulate the SIS junctions, we took the following physical effects into account: the proximity effect, dumping factor, impurity band, and Ohmic resistance. These defects are explained in the following sections.

4.1 Proximity Effect

It is known that a thin layer of normal metal becomes a superconductor if it is attached to a superconductor. This phenomenon is called the proximity effect [9]. The gap energy of the superconductor and the normal metal in the proximity effect can be expressed as follows [9]:

$$\varDelta_N(E) = \left(\varDelta_N^0 + \frac{\varGamma_N \varDelta_S(E)}{\sqrt{\varDelta_S(E)^2 - E^2}}\right) \Bigg/ \left(1 + \frac{\varGamma_N}{\sqrt{\varDelta_S(E)^2 - E^2}}\right), \tag{4}$$

and

$$\varDelta_S(E) = \left(\varDelta_S^0 + \frac{\varGamma_S \varDelta_N(E)}{\sqrt{\varDelta_N(E)^2 - E^2}}\right) \Bigg/ \left(1 + \frac{\varGamma_S}{\sqrt{\varDelta_N(E)^2 - E^2}}\right), \tag{5}$$

where Δ_S^0 and Δ_N^0 are the original gap energy of the superconductor and normal metals, respectively, and $\varGamma_N = \hbar/\tau_N$ and $\varGamma_S = \hbar/\tau_S$, where τ_S and τ_N are the relaxation times of the superconductive and normal metals, respectively.

4.2 Damping Factor

The damping effect can be taken into account if an imaginary part of the gap energy is introduced [7]:

$$\varDelta_S^0 = \varDelta_1(1 + i\varDelta_2), \tag{6}$$

In this case, Δ_2 is a phenomenological parameter that can broaden the sharp transition at the gap edge in the state density. The broadening of the density of state may be caused by the non-uniformity and anisotropy of superconductivity.

4.3 Impurity Band

It has been reported that the sub-gap current in some SIS junctions is enhanced above half of the gap voltage [7]. To explain this, an impurity band was introduced. The impurity band grows along with an increase in the concentration of spins due to magnetic impurities (Fe, Mn, Cr) [10] in the superconductor. Noguchi *et al.* [7] suggested that this type of localized impurity band can be accommodated by adding the following term into Eq. (2):

$$c\left\{\frac{a}{(E-b)^2 + a^2} + \frac{a}{(E+b)^2 + a^2}\right\}, \tag{7}$$

where a, b, and c are parameters representing the width, peak energy, and amplitude of the impurity band, respectively.

4.4 Ohmic Resistance

The sub-gap current of the IV curves of the SIS junctions sometimes show linear increases in the voltage. We assumed that this was caused by the Ohmic currents generated by the defects and normal-conducting channels of the normal metal embedded in the insulator. We therefore introduced a conductance parameter $1/R$ to represent the Ohmic current, and we then added a V/R term to the right-hand side of Eq. (1).

4.5 The Equations Used for the Fittings

In summary, we used the following equations to fit the IV curves:

$$I_T(V) = A \int N_u(E - eV) N_l(E) \times \{f_u(E - eV) - f_l(E)\} dE + \frac{V}{R}, \tag{8}$$

and

$$N_{u,l}(E) = \mathrm{Re}\left[\frac{|E|}{\sqrt{E^2 - {\Delta_{u,l}}^2}}\right] + c\left\{\frac{a}{(E-b)^2 + a^2} + \frac{a}{(E+b)^2 + a^2}\right\}. \tag{9}$$

In the above equations, $\Delta_{u,l}$ can be calculated from Eqs. (4), (5), and (6). During the fitting process, the temperature T was fixed at 4.2 K, and $\varDelta_N^0$ was assumed to be zero. Consequently, there are a total of eight free parameters ($\varDelta_1$, $\varDelta_2$, $\varGamma_S$, $\varGamma_N$, a, b, c, and $1/R$) in the fitting process.

4.6 Results of the Fittings

Figure 4 shows the results of the model fitting, and the fitted parameters are summarized in Table 1. For comparison, we also plotted the ideal IV curves calculated with the Bardeen–Cooper–Schrieffer (BCS) density of states. In Fig. 4, we can see that both of the IV curves are well described by the present model. In the case of the Nb/Al/AlO_x/Al/Nb junction, we found that the degradation of the sub-gap current in the voltage range from 1.5–2 mV was not dominated by the Ohmic current but by the current contribution from the gap broadening and impurity band.

The following three subjects should be discussed based on our comparison of the fitted parameters. First, the Ohmic conductance $1/R$ of the Nb/Al/AlO_x/Al/Nb junction is much

Table 1 Fitting parameters.

	Top Layer				Bottom Layer				a	b	c	$1/R$
	Δ_1	Δ_2	Γ_N	Γ_S	Δ_1	Δ_2	Γ_N	Γ_S				
Nb/Al/AlO_x/Al/Nb	1.305	0.008	33.0	0.05	1.305	0.008	5.50	0.05	0.25	0.45	0.0025	< 0.003
Nb/Al/AlO_x/Nb	1.360	0.015	-	-	1.305	0.008	5.30	0.10	0.25	0.45	0.0025	0.06

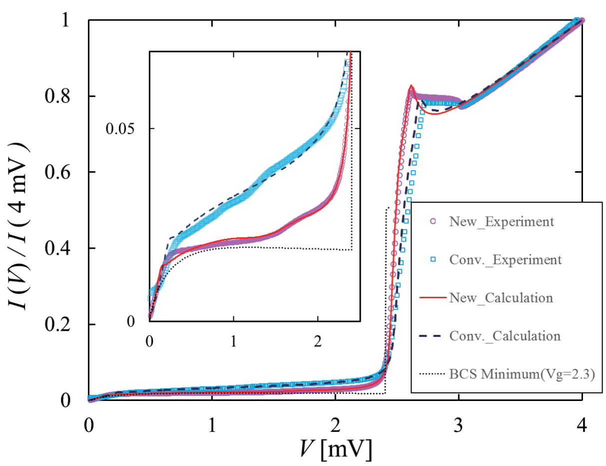

Fig. 4 Results of the fittings to the *IV* curves for the Nb/Al/AlO_x/Nb junction (blue squares) and the Nb/Al/AlO_x/Al/Nb junction (yellow circles). The solid and dashed lines are the fitted results for the Nb/Al/AlO_x/Al/Nb junction and the Nb/Al/AlO_x/Nb junction, respectively. The dotted line is the one calculated from the ideal BCS theory.

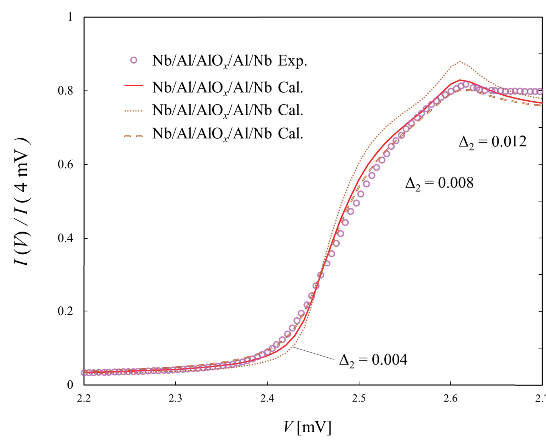

Fig. 5 Changes in the *IV* characteristics just below the gap voltage of the Nb/Al/AlO_x/Al/Nb junction with respect to the magnitude of Δ_2.

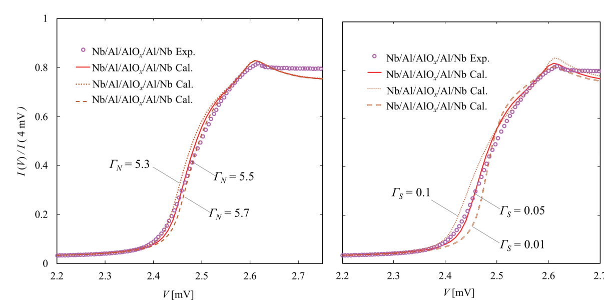

Fig. 6 Changes in the *IV* characteristics near the gap voltage of the Nb/Al/AlO_x/Al/Nb junction with respect to (a) Γ_N and (b) Γ_S.

lower than that of the Nb/Al/AlO_x/Nb junction. In the case of Nb/Al/AlO_x/Al/Nb junction, the Ohmic conductance was not considered because it was assumed to be negligibly small $< 0.003\ \Omega^{-1}$ based on the slope of the sub-gap current of the measured *IV* curve. Moreover, we found that the leakage current was proportional to the junction area by evaluating the current measured in junctions with diameters of 2, 1.5, and 1 μm. These results indicate that the leakage current is caused by defects in the insulator and that it is very low in the Nb/Al/AlO_x/Al/Nb junction.

Second, the dumping factor of the top electrode in the Nb/Al/AlO_x/Al/Nb junction was also lower than that of the Nb/Al/AlO_x/Nb junction. Figure 5 shows examples of the changes in the *IV* curves just below the gap voltage with respect to Δ_2. The change of the *IV* curves with respect to this range of Δ_2 was sufficiently large that there was a significant difference in Δ_2 between the Nb/Al/AlO_x/Al/Nb and Nb/Al/AlO_x/Nb junctions. Since the dumping factor was assumed to be caused by existing lower gap-voltage superconductors (i.e. NbO_x) embedded in the Nb near the AlO_x, this suggests that the creation of degraded superconductors with lower gap voltages was sufficiently suppressed in the Nb/Al/AlO_x/Al/Nb junction as compared to the Nb/Al/AlO_x/Nb junction.

Third, the proximity effect in the bottom electrode of the Nb/Al/AlO_x/Nb junction appears to be stronger than that of the Nb/Al/AlO_x/Al/Nb junction, based on a comparison of the Γ_N and Γ_S parameters. Figure 6 shows examples of the changes in the gap voltage with respect to Γ_N and Γ_S. In Fig. 6 (a) it can be seen that the magnitude of the gap voltage was mainly determined by Γ_N, and in Fig. 6 (b) it can be seen that the slope of the current step at the gap voltage was mainly determined by Γ_S. As the strength of the proximity effect increased, Γ_N and Γ_S decreased and increased, respectively. Thus, the proximity effect in the bottom electrode of the Nb/Al/AlO_x/Nb junction was considerably stronger than that of the Nb/Al/AlO_x/Al/Nb junction. This degradation is thought to be caused by the excess diffusion of the top Nb into the bottom Al through the AlO_x, which was sufficiently suppressed by the top Al layer in the Nb/Al/AlO_x/Al/Nb junction. We believe that there are two reasons why the diffusion of the Nb into the Al enhances the proximity effect.

One reason is that the diffused Nb could convert into NbO_x, which gives the anisotropy of superconductivity. The other reason is that the Al layer involves the diffused NbO_x which may significantly reduce the mean free pass of the quasiparticles in the Al layer and may also increase the Γ_N.

Furthermore, the current in the voltage of < 1 mV for the Nb/Al/AlO_x/Al/Nb junction had approximately the same magnitude as that calculated using the BCS density of states. This result indicates that the quality of the AlO_x insulator was close to ideal. Therefore, it is most likely that the extra Al layer on top of the AlO_x layer effectively suppressed not only the diffusion of Nb into the AlO_x and bottom Al layers, but also suppressed the creation of defects and/or conductive channels in the AlO_x caused by the reaction of the Nb with the AlO_x.

5. Observations of SIS Cross Sections

In this section, we directly observe and compare the microscopic structure of the two junctions by using the Energy Dispersive X-ray spectrometry (EDX) and Scanning Transmission Electron Microscope (STEM) images. In Fig. 7, the STEM images of the cross section for the Nb/Al/AlO_x/Al/Nb and Nb/Al/AlO_x/Nb junctions are shown. In the image of the Nb/Al/AlO_x/Al/Nb junction, the top Al layer is slightly brighter than the bottom Al layer, and there is a spatial variation of the brightness in the top Al layer. This variation may be caused by the existence of Nb in the top Al layer. In fact, the abundance of Nb in the top Al layer is 5–8% larger than in the bottom Al layer, based on the EDX line analyses shown in Fig. 8 (a). On the other hand, it is clear that the bottom Al layer contains a significant amount of Nb, as shown in Fig. 8 (b).

In Figs. 7 (a) and (c), the points at which the EDX point analyses were performed are indicated by Labels 1-1 and 1-2 for the top and bottom Al layers in the Nb/Al/AlO_x/Al/Nb junction, respectively, as well as by Label 2 for the bottom Al layer of the Nb/Al/AlO_x/Nb junction for comparison. The EDX profiles of those points are shown in Fig. 9. It can be seen that in the Nb/Al/AlO_x/Al/Nb junction, the absolute quantity of Nb in the top Al layer was larger than that in the bottom Al layer. It can also be seen in Fig. 9 (b) that only a small amount of Nb was involved in the bottom Al layer in the Nb/Al/AlO_x/Al/Nb junction. On the other hand, it can be seen in Fig. 9 (c) that a significant amount of Nb was present in the bottom Al layer of the Nb/Al/AlO_x/Nb junction. Since the deposition procedure and growth conditions of the bottom Al and AlO_x layers on the bottom Nb for both types of junctions were approximately the same, the Nb in the bottom Al layer of the Nb/Al/AlO_x/Nb junction must have come from the top Nb, especially during the deposition process. Thus, we believe that the top Al layer protected against the diffusion of Nb into the bottom Al layer, although a small number of Nb atoms were able to diffuse into the top Al layer.

In the STEM image of the Nb/Al/AlO_x/Nb junction shown in Fig. 7 (d), a contrast of the brightness can be seen in the bottom Al layers. This indicates that the Nb penetrated not only into the AlO_x insulator but also into the bottom electrode. Consequently, a large number of defects

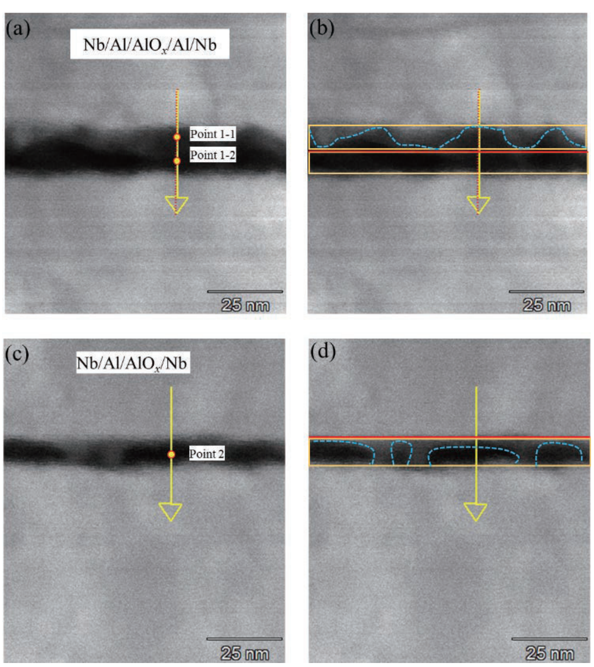

Fig. 7 (a) and (b) STEM images of the Nb/Al/AlO_x/Al/Nb junction, and (c) and (d) are those of the Nb/Al/AlO_x/Nb junction. In (b) and (d), the red solid lines and yellow rectangles indicate the AlO_x and Al layers, respectively, and the blue dashed lines show the difference of contrast in the Al layers. The yellow arrows indicate the areas in which the EDX analyses shown in Fig. 8 was performed. The yellow points indicate the points at which the EDX point analyses shown in Fig. 9 was carried out.

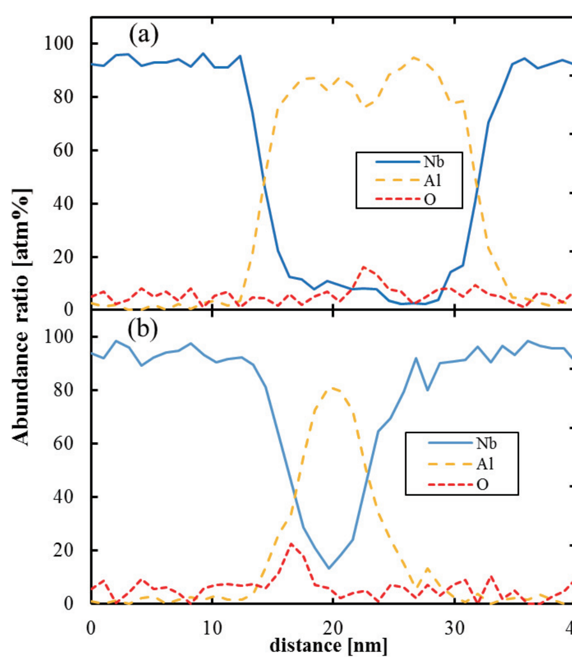

Fig. 8 Profiles of the EDX line analyses for (a) the Nb/Al/AlO_x/Al/Nb junction and (b) the Nb/Al/AlO_x/Nb junction.

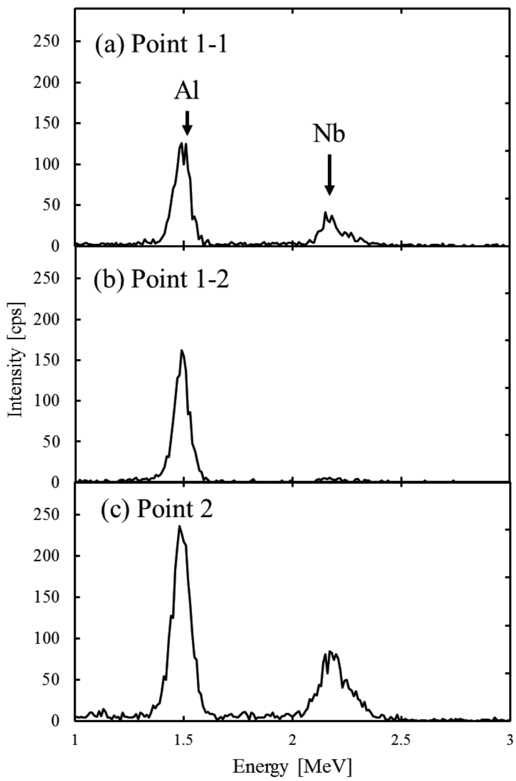

Fig. 9 EDX spectra of Nb and Al for (a) top and (b) bottom Al layers of the Nb/Al/AlO$_x$/Al/Nb junction and (c) for bottom Al layer of the Nb/Al/AlO$_x$/Nb junction.

were created in the AlO$_x$ insulator in the Nb/Al/AlO$_x$/Nb junction. Thus, we conclude that the extra Al layer on top of the AlO$_x$ insulator is required for high quality J_c SIS junctions with a high critical current density in order to protect the extremely thin insulator from being damaged.

6. Conclusions

We have determined that the sub-gap leakage current of the Nb/Al/AlO$_x$/Al/Nb junction is much lower than that of the Nb/Al/AlO$_x$/Nb junction. Based on our fitting of the *IV* curves, we found that the sub-gap leakage current in the Nb/Al/AlO$_x$/Nb junction is likely due to the conduction channels (e.g. normal metal, such as Al or NbO$_x$) embedded in the insulator, and that such defects can be suppressed by introducing an extra Al layer. From the STEM images and EDX analyses, we confirmed that Nb atoms do not reach the bottom electrode in the Nb/Al/AlO$_x$/Al/Nb junction. Thus, the Nb/Al/AlO$_x$/Al/Nb junctions will be suitable for use in high critical current density junctions. Furthermore, an extra Al buffer layer is also useful for other type of high J_c SIS junctions, such as Nb/Al/AlN$_x$/Al/Nb junctions.

Acknowledgments

The authors would like to thank Ms. Yumi Fujii for her invaluable support during the fabrication of the SIS junctions, and Dr. Matthias Kroug for his insightful comments and suggestions. We would also like to thank Assoc. Prof. Shan Wenlei for carefully reading this manuscript and providing valuable comments. This work was carried out in collaboration with the Advanced Technology Center (ATC) at NAOJ, and we would like to thank all members in the ATC. This study was supported by KAKENHI (25108005, 25400225 and 26420330).

References

[1] Y. Uzawa, M. Kroug, T. Kojima, M. Takeda, M. Candotti, Y. Fujii, K. Kaneko, W. Shan, T. Noguchi, and Z. Wang, “A sensitive ALMA band 10 SIS receiver engineering model,” Supercond. Sci. Technol., vol.22, no.11, p.114002, 2009.

[2] A. Endo, AlN tunnel barriers for submillimeter wave SIS mixers, Ph.D. thesis, Dept. Astron., Tokyo Univ., Tokyo, Japan, 2009.

[3] M. Ohkubo, S. Shigetomo, M. Ukibe, G. Fujii, and N. Matsubayashi, “Superconducting tunnel junction detectors for analytical sciences,” IEEE Trans. Appl. Supercond., vol.24, no.4, Aug. 2014.

[4] M. Gurvitch, J.M. Rowell, H.A. Huggins, M.A. Washington, and T.A. Fulton, “Nb Josephson tunnel junctions with thin layers of Al near the barrier,” IEDM-81, pp.115–117, 1981.

[5] A. Zehnder, P. Lerch, S.P. Zhao, T. Nussbaumer, E.C. Kirk, and H.R. Ott, “Proximity effects in Nb/Al-AlO$_x$-Al/Nb superconducting tunneling junctions,” Phys. Rev. B, vol.59, no.13, pp.8875–8886, 1999.

[6] S. Morohashi, T. Miyoshi, Y. Takada, C. Yamamoto, H. Matsuo, A. Kushino, and M. Ohkubo, “Characteristics of Nb/Al-AlOx-Al/Nb Josephson junction fabricated using facing target sputtering,” Journal of Physics: Conference Series, vol.43, pp.1100–1104, 2006.

[7] T. Noguchi, T. Suzuki, and T. Tamura, “Subgap tunneling current at low temperature in Nb/Al-AlN/Nb SIS junctions,” IEEE Trans. Appl. Supercond., vol.21, no.3, pp.756–759, 2011.

[8] M. Tinkham, Introduction to Superconductivity, 2nd ed., Dover Publishing, New York, 2004,

[9] W.L. MacMillan, “Tunneling model of the superconducting proximity effect,” Phys. Rev., vol.175, no.2, pp.537–542, 1968.

[10] H. Shiba, “Classical spins in superconductors,” Progress of Theoretical Physics, vol.40, no.3, pp.435–451, 1968.

Mizuki Ikeya received B.E. and M.E. degrees in the Department of Communications Engineering and Informatics from the University of Electro-communications in 2014 and 2016, respectively.

Takashi Noguchi was born in Saitama, Japan, on April 3, 1952. He received the B.S., M.S. and Ph.D. degrees in applied physics from Tohoku University, Sendai, Japan, in 1976, 1978 and 1981, respectively. In 1981 he joined the Central Research Laboratory, Mitsubishi Electric Corporation, where he was engaged in the research and development of superconducting devices for analog applications. He left Mitsubishi Electric Corporation in 1991 to join Nobeyama Radio Observatory, National Astronomical Observatory of Japan (NAOJ). In 2005, he moved to Advanced Technology Center of NAOJ to carry out the development of low-noise receivers for the telescopes of Atacam Large Millimeter/submillimeter Array (ALMA). His current research interest is the development of low-noise SIS mixers for the THz frequency band.

Takafumi Kojima received the B.S., M.S. and D.S. degrees in physics from the Osaka Prefecture University, Osaka, Japan, in 2005, 2007, and 2010, respectively. He is currently an Assistant Professor at the Advanced Technology Center, National Astronomical Observatory of Japan, Mitaka, Japan. His research interests are in the area of superconducting RF circuit.

Takeshi Sakai received a B.S. from the Tokyo Institute of Technology, Tokyo, Japan, in 1999. He received M.S. and Ph.D. degrees from the University of Tokyo in 2001 and 2004, respectively. In 2014, he joined the Graduate School of Informatics and Engineering at the University of Electro-Communications as an assistant professor.